Experimental Verification of a Generalized Multivariate Propagation Model for Ionospheric HF signals

Y. Abramovich†
Odessa State Polytechnic University
av. Shevchenko 1, 270044, Ukraine
Tel +38 0482 288644

C. Demeure
THOMSON-CSF Division Communication
66 rue du Fossé Blanc, 92231, Gennevilliers, France.
Tel: (33)1-46132113; Fax (33)1-46132555

A. Gorokhov†
Télécom Paris, Dépt. Signal
46 rue Barrault
75634 Paris Cedex 13 FRANCE

ABSTRACT

New stochastic model for HF signal, received by the multisensor antenna array is presented for ionospheric propagation channel. The model introduces spatial fluctuations that are observed by the receiving antenna array, along with the Doppler frequency fluctuations. The new description generalizes the existing models and collapses into the perfectly validated scalar Watterson model for the single sensor reception. The proposed model is stimulated by practical attempts to improve the performance of HF radiosystems, and has been validated by the set of experimental transmissions from Coloumier (France), received by the antenna array in Odessa (Ukraine). Experimental results demonstrate a good compliance with the introduced model.

1 INTRODUCTION

Spatial diversity of the HF signals, received by multisensor antenna arrays, is under exploration nowadays for the performance improvement of the radio systems, such as HF modems or OTH radars.

Recent attempts to introduce the spatial adaptive beamforming for the signal sub-interference visibility improvement revealed the essential spatial fluctuations observed by receiving antenna over the typical dwells [1].

While the Doppler fluctuations introduced by ionospheric channels have been widely investigated and are reflected by existing models, spatial fluctuations have not been introduced so far. For example, under the Watterson multivariate model [1] a signal wavefront is supposed to be time-independent and defined by the signal direction of arrival (DOA) only.

Another model [2] adopts deterministic description of the Doppler frequency modulation, different for ordinary and extra-ordinary components. Once again, this model presumes that correspondent wavefronts for each component are rigid over arbitrary long observation interval.

Thus, in accordance with existing models the eigensubspace of the N-variate spatial covariance matrix has to have a fixed signal subspace dimension regardless to the observation period used for averaging.

Of course, even the shortest observation interval discussed is long enough as compared to the Nyquist rate, to neglect finite sample size considerations. Experiments discussed below have demonstrated contradictions between above mentioned theoretical models and the actual spatial properties.

2 EXPERIMENTAL RESULTS

Antenna array of 8 sensors, supplied by the coherent 8-channel HF receiver, has been used. The sampling rate of 11-bit analog-to-digit convertor (ADC) of the real and imaginary component of the signal was nominally equal to $_{\vartriangle}F = 10$ kHz, matched with IF bandwidth.

By calibration procedure, described in [4] the maximum ratio between two dominant eigenvalues was defined as $18 - 19$ dB, for true single broadband source irradiated from the near-field. This ratio does not depend on the signal-to-noise ratio, and is defined by nonidentity of the transfer functions of the multichannel receiver, that has been used in experiment. For narrowband sources ($_{\vartriangle}F = 2.4$ kHz) this ratio is slightly better, $21-22$ dB. This dynamic range was sufficient enough in many cases to observe the spatial nonstationarity phenomenon.

Table 1 illustrates the eigendecomposition of quasi-instanteneous sample covariance matrices, estimated along an observation interval of 40 sec for the bandwidth $_{\vartriangle}F = 10$ kHz. One can see that the broadcasting signal is "seen" by the system as a narrowband with undoubtfully defined spatial rank, equal to one, for each quasi-instanteneous interval. Table 2 correspondes to the same scenario, when these quasi-instanteneous matrices have been consequently averaged. Degradation of spatial properties, caused by the growth of signal subspace dimension for the averaged matrix, is quite obvious. Note, that not at all each ionospheric trial exhibits such property and this phenomenon has been never observed for the ground-wave propagated signals.

Experiments for simultaneous spatial and temporal (Doppler) fluctuations have been conducted with the HF modem signal ($_{\vartriangle}F = 2,4$ kHz), transmitted from Coloumier and received by Odessa facility. Linear antenna array of this facility is in "end-fire" orientation towards the transmission point. With respect to the modest aperture ($\sim$ 200 m), spatial diversity for the testing signal was minimized, being arbitrary for the "signals of opportunity".

Typical behaviour of two largest eigenvalues of the covariance matrix for the interference source observed along with the useful signal is demonstrated by Fig. 1. Eigendecomposition for the quasi-instanteneous (solid

†This work was supported in part by the French DRET administration and in part by SASPARC project of INTAS and SOROS grants.

line) and averaged (dashed line) covariance matrices has been performed.

One can see, that nonstationarity leads to $\sim 15-20$ dB degradation here, where the observation interval was equal to 40 sec. Note that for the wideband (10 kHz) scenario this phenomenon is usually much more profound.

Similar ratio for the extracted dominant spatial mode of the testing signal emitted from Coloumier, is illustrated by Fig. 2. One can see, that spatial nonstationarity of this signal is less emphasized. Doppler spectrum of this mode is illustrated by Fig. 3. Thus, for different angle of signal arrival we were able to observe the different "bandwidth" of spatial fluctuations.

3 GENERALIZED WATTERSON MODEL

To modify the existing Watterson model in the simpliest way, the following generalization has been proposed. The signal, irradiated by some given source is presented at the N-element antenna input as a sum of p modes:

$$X(t) = \sum_{m=1}^{p} X_m(t) + \eta(t), \qquad 0 < t < T_{obs}, \quad (1)$$

$$X_m(t) = a_m\, S(\mu_m)\, C_m(t,\mu_m)\, u(t-\tau_m)\, e^{i\Delta\omega_{0m}\, t}. \quad (2)$$

Here $S(\mu_m) \triangleq \mathrm{diag}\,\{S_k(\mu_m)\}_{k=1}^{N}$ is the N-dimensional diagonal matrix formed by the m-th mode "steering vector", defined by the DOA μ_m; ω_{0m} is the regular component of the ionospheric Doppler shift for the m-th mode, τ_m is a correspondent group delay, a_m is the RMS value of the m-th mode amplitude, and $\eta(t)$ is an additive white noise of the power σ^2,

$$\mathbb{E}\left\{\eta(t_1)\,\eta(t_2)^H\right\} = \sigma^2\,\delta(t_1,t_2)\,\mathrm{I}_N, \quad (3)$$

$u(t)$ is the transmitted waveform, as usual. Spatial and temporal fluctuations are introduced by the two-dimensional (space-temporal) random N-element vector $C_m(t,\mu_m)$.

Temporal sequence $C_m(t,\mu_m)$ is described by the multivariate AR model:

$$C_m(t,\mu_m) = -\sum_{i=1}^{l} \rho_m(iT_r)\, C_m(t-iT_r,\mu_m) \quad (4)$$

$$+\alpha_m\, \varepsilon^{(m)}(t),$$

where the scalar AR coefficients $\rho_m(iT_r)$ are defined by the standard assumptions on the Doppler power spectrum. The example illustrated by Fig. 3. should be obviously described by the AR model of the second order ($l=2$). To introduce spatial fluctuations, the simpliest Markov model can be adopted

$$\varepsilon_{i+1}^{(m)}(t) = r^{(1-|\sin\mu_m|)}\,(d_{i+1}-d_i)\,\varepsilon_i^{(m)}(t) + \quad (5)$$

$$\sqrt{1-|r^{(1-|\sin\mu_m|)}\,(d_{i+1}-d_i)|^2}\;\gamma_{i+1}^{(m)}(t),$$

where $d_{i+1}-d_i$ is the antenna inter-element distance, and $r^{(1-|\sin\mu_m|)}\,(d_{i+1}-d_i)$ is the correspondent spatial correlation coefficient. One can see, that depending on μ_m, this coefficient may change from some $r<1$ (for $\mu_m=0$) to $r\to 1$ for the endfire signal DOA ($\mu_m \to \frac{\pi}{2}$):

$$r(d_{i+1}-d_i) = e^{-D\,|d_{i+1}-d_i|}. \quad (6)$$

For the arbitrary antenna weight vector W, the scalar output signal is now described by the well-approved scalar Watterson model. We presume, that observation interval T_{obs} is supposed here to be short enough to ignore the DOA regular transformation.

Under the introduced model the spatial covariance matrix of the given mode may be presented as a Shur-Hadamard product:

$$R(\mu_m) = (S(\mu_m)\,S(\mu_m)^H) \otimes B(\mu_m), \quad (7)$$

where the symbol $\otimes$ means the element-wise product,

$$B(\mu_m) = \left[e^{-D\,(1-|\sin\mu_m|)\,|d_i-d_j|}\right]_{i,j=1}^{N}. \quad (8)$$

Meanwhile, it is clear now that any quasi-instanteneous sample covariance matrix for the given mode m, is of the first rank over the intervals comparable with the frame duration, since for typical Doppler spectra

$$\rho_1(0.01\mathrm{sec}) \to 1; \qquad \rho_{2,\ldots,l} \to 0. \quad (9)$$

On the other hand, when $T_{obs}\to\infty$, the spatial sample covariance matrix falls into its limit (7).

In order to demonstrate the efficiency of the introduced model, Table 3 illustrates the results of stochastic simulation for the single mode propagated signal with the following parameters for a uniform antenna array:

$$r^{(1-\sin\mu)}(|d_{i+1}-d_i|) = 0.9, \qquad i=1,\ldots,N-1,$$

$$l=1, \qquad \rho_1(\tau) = e^{-B|\tau|}, \qquad B = 0.5\mathrm{Hz}.$$

Table 3 illustrates the averaged eigenvalues of the quasi-instanteneous ($T=0$) sample matrices (first row) and the eigenvalues of the covariance matrix, averaged over entire observation interval ($T=40$ sec). The coincidence of the simulated and experimental results (Table 1) is quite remarkable. Note that the model introduced, as well as the previous ones [2, 3] assume an ideal plane wave antenna manifold. For many applications "mean" wavefront could not be simply defined by the linear front. The following generalization, based on the Karhunen-Loeve expansion, may be proposed,

$$X_m(t) = \alpha_m\, F(\mu_m)\, C_m(t,\mu_m)\, u(t-\tau_m)\, e^{i\Delta\omega_{0m}\, t}, \quad (10)$$

$$F_m(\mu_m) = V(\mu_m)\,\Lambda_m^{\frac{1}{2}}; \quad (11)$$

$$R(\mu_m) = V(\mu_m)\,\Lambda\,V(\mu_m)^H. \quad (12)$$

Similarly to (7), $R(\mu_m)$ correspondes to the sample matrix, averaged over the observation interval T_{obs}, long enough to have $T_{obs}\,B \gg N$, for example. By these results, the general model with the spatial wavefront fluctuations, linked with the temporal (Doppler) fluctuations is introduced. Spatial fluctuations bandwidth depends on the effective antenna aperture (angle of arrival) and usually increases when the Doppler spread bandwidth increases.

References

[1] Rapport CCIR no 594-2, "Simulations of Ionospheric channels for decametric waveform".

[2] L. Bertel, Conrvez P.Rojas Varela J. "Modèle analytique de signaux HF après propogation par voie ionospherique". Note technique NT/LAB/ MER 225, CNET (1986).

[3] Y. Abramovich *et al.* , "Experimental efficiency research of adaptive spatial unpremediated noise compensation in HF radars for distance sea surface diagnostics", Radiotechnika i Electronika, vol 38(4) pp. 664-671, 1993 (in Russian).

[4] Y. Abramovich *et al.* , "The Effectiveness of Spatial Interference Compensation in Systems with Nonidentical Reception Channels", Soviet Journal of Communications Technology and Electronics, 1990 v. 35 No 2 pp. 96-104.

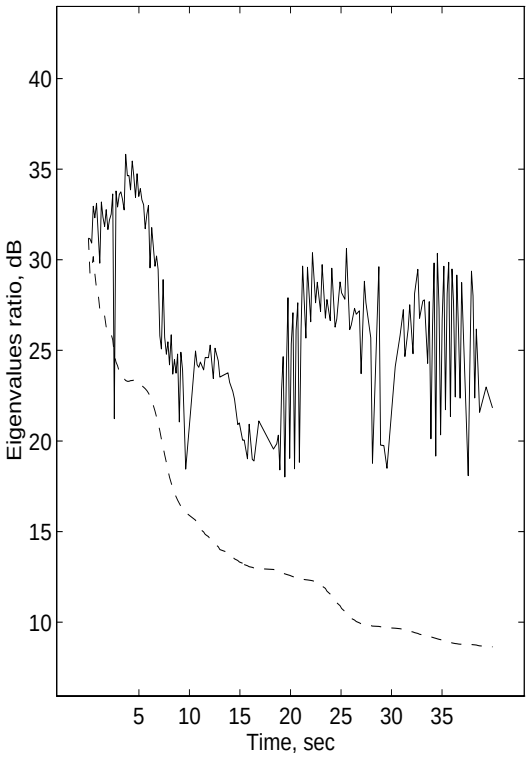

Fig.1. Eigenvalues ratio:
" - ": quasi-instantaneous, "- -": average.

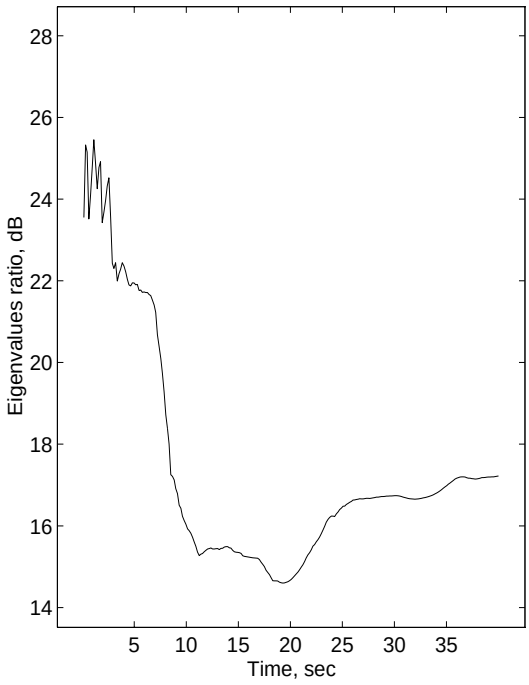

Fig.2. Eigenvalues ratio:
" - ": quasi-instantaneous, "- -": average.

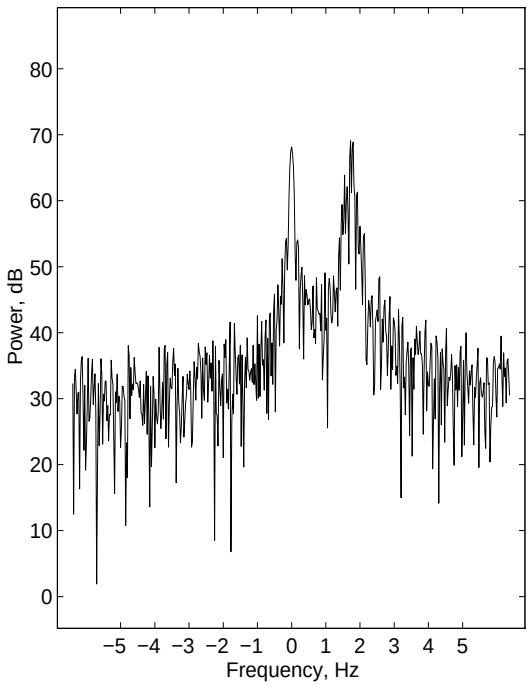

Fig.3. Doppler power spectrum.

Table 1

T sec	Eigenvalues, dB with respect to the main one							
0	0	-22.6	-26.7	-28.7	-33.4	-37.1	-38.8	-40.3
1	0	-20.3	-29.6	-34.7	-36.2	-38.6	-40.0	-44.0
2.5	0	-14.7	-21.4	-25.8	-29.1	-32.4	-34.0	-37.0
5	0	-12.5	-18.2	-32.1	-36.3	-38.4	-39.8	-41.1
7.5	0	-31.7	-33.1	-35.3	-37.6	-39.0	-41.5	-42.9
10	0	-17.4	-24.9	-30.9	-33.9	-38.1	-40.4	-42.8
12.5	0	-13.2	-17.6	-28.7	-29.8	-33.4	-36.4	-39.4
15	0	-10.0	-18.7	-25.9	-28.5	-30.3	-32.5	-37.0
20	0	-26.6	-29.9	-32.8	-35.2	-37.4	-40.4	-42.6
25	0	-34.3	-36.0	-37.0	-37.9	-39.8	-42.3	-46.1
30	0	-29.2	-30.5	-32.2	-35.1	-37.7	-40.1	-42.0
35	0	-13.6	-18.1	-23.1	-30.6	-33.7	-37.2	-38.3
40	0	-24.4	-29.8	-31.0	-32.5	-34.5	-35.8	-40.2

Table 2

T sec	Eigenvalues, dB with respect to the main one							
0	0	-22.6	-26.7	-28.7	-33.4	-37.1	-38.8	-40.3
1	0	-8.9	-21.7	-29.1	-31.4	-35.3	-36.6	-39.8
2.5	0	-7.8	-10.7	-15.9	-22.3	-25.9	-30.1	-33.6
5	0	-5.8	-8.3	-13.6	-16.4	-20.2	-24.4	-25.2
7.5	0	-5.9	-7.9	-12.0	-15.4	-19.5	-22.0	-25.2
10	0	-4.9	-7.5	-9.7	-15.0	-18.6	-22.0	-23.6
12.5	0	-4.3	-6.7	-9.0	-13.0	-17.5	-20.5	-22.9
15	0	-4.3	-7.2	-8.7	-12.9	-17.6	-20.3	-22.9
20	0	-4.5	-6.4	-8.5	-12.1	-17.7	-19.8	-22.2
25	0	-4.3	-6.1	-8.4	-12.2	-17.3	-19.4	-21.9
30	0	-4.1	-6.2	-9.0	-12.4	-17.5	-19.7	-22.2
35	0	-4.8	-6.7	-9.2	-12.7	-17.9	-20.1	-22.5
40	0	-4.9	-6.5	-8.9	-12.2	-17.8	-20.1	-22.4

Table 3

T sec	Eigenvalues, dB with respect to the main one							
0	0	-18.1	-21.7	-25.7	-31.4	-34.1	-39.1	-41.2
40	0	-17.9	-20.9	-25.2	-30.9	-34.0	-38.1	-41.4